PAPER

Two magnetic Δ-chain-based Mn(II) and Co(II) coordination polymers with mixed carboxylate–phosphinate and μ₃-OH⁻ bridges†

Zi-Yi Du,[a] Ling Zhang,[a] Bao-Ying Wang,[b] Sui-Jun Liu,*[c] Bo Huang,[b] Cai-Ming Liu*[d] and Wei-Xiong Zhang*[b]

The hydrothermal reaction of Mn(II) or Co(II) ions with 2-carboxyethyl(phenyl)phosphinic acid (H_2L) afforded Mn(II) and Co(II) carboxylate–phosphinates containing μ₃-OH⁻ as a co-ligand, namely $[M_3(L)_2(OH)_2]$ (M = Mn (**1**) or Co (**2**)). Such two compounds feature a new layered structure in which Δ-type chains built from alternating corner- and edge-sharing $M_3(μ_3$-OH) triangles are further connected *via* the Y-shaped "–(CH₂)₂–C(–O–)–" spacers. Magnetic studies reveal that there are dominant antiferromagnetic interactions between the metal ions. In **1**, the complicated magnetic couplings in the Δ-type chains result in spin competition, displaying spin-glass behaviors. In **2**, spin fluctuation behavior was observed and the critical field at 2 K is 25 kOe.
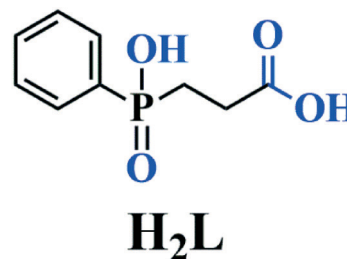
Introduction

During the past few decades, molecule-based magnetic materials with rich magnetic couplings have attracted considerable attention in coordination chemistry, owing to their intriguing magnetic phenomena as well as their potential applications in quantum computation and information storage.[1–3] Among the classes of magnetic materials, frustrated magnets and spin fluctuation complexes are of particular theoretical interest.

On the one hand, in frustrated magnets, localized magnetic moments, or spins, interacting through competing exchange interactions cannot be simultaneously satisfied, which may lead to some interesting phenomena such as spin liquid at low temperature.[4] As one of the archetypes of spin frustration, Δ-type chain magnets that contain chains of corner- and/or edge-sharing triangles of $M_3(μ_3$-bridge) may provide a theoretical model to study magneto-structural correlations and act as secondary building blocks to construct novel frustrated materials. However, up to now, examples of coordination polymers (CPs) with Δ-type chain structures are still limited in number.[5–7] To create magnetic CPs with Δ-type chain structures, the introduction of a μ₃-OH⁻ co-ligand has been proved to be an effective strategy.

On the other hand, metamagnetic or spin fluctuation behaviour may occur if the couplings are weak enough to be overcome by an external field and enter into another magnetic state along with the reorientation of spin.[8] Frequently, such couplings are not strong and are exhibited in inter-molecule, interchain, and interlayer interactions mediated by long linkers, blocking groups, hydrogen bonds, and π–π interactions.[8a,9]

Recently, we have undertaken research works on the coordination chemistry of a bifunctional ligand, namely 2-carboxyethyl(phenyl)phosphinic acid (H_2L, see Scheme 1), which features two formally analogous carboxylate and phosphinate moieties (*i.e.*, both contain two potential O donors) separated by a flexible ethylene spacer. The use of such

[a] *College of Chemistry and Chemical Engineering, Gannan Normal University, Ganzhou 341000, China*

[b] *School of Chemistry, Sun Yat-Sen University, Guangzhou 510275, China. E-mail: zhangwx6@mail.sysu.edu.cn*

[c] *School of Metallurgy and Chemical Engineering, Jiangxi University of Science and Technology, Ganzhou 341000, China. E-mail: liusuijun147@163.com*

[d] *Beijing National Laboratory for Molecular Sciences, Center for Molecular Science, Institute of Chemistry, Chinese Academy of Sciences, Beijing 100190, China. E-mail: cmliu@iccas.ac.cn*

† Electronic supplementary information (ESI) available: PXRD patterns, TGA curves and magnetic characterization of **1** and **2**. CCDC 1054109 and 1418238. For ESI and crystallographic data in CIF or other electronic format see DOI: 10.1039/c6ce02537d

Scheme 1 Structure of the ligand H_2L used for the construction of **1** and **2**.

a conformationally flexible ligand with multiple donor sites has demonstrated the structural diversity for the construction of CPs.[10,11] In our current studies on magnetic CPs of metal carboxylate–phosphinates, here we present two unique examples of magnetic materials with Δ-type chain structures, i.e. [Mn₃(L)₂(OH)₂] (**1**) and [Co₃(L)₂(OH)₂] (**2**). Herein, we report their syntheses, crystal structures, and magnetic properties.

Experimental

Materials and instrumentation

2-Carboxyethyl(phenyl)phosphinic acid was prepared using a published procedure.[12] All other chemicals were obtained from commercial sources and used without further purification. FT-IR spectra were recorded on a Nicolet 5700 spectrometer using KBr pellets in the range of 4000–400 cm^{-1}. Powder X-ray diffraction (PXRD) patterns (Cu-Kα) were collected on a Bruker Advance D8 θ–2θ diffractometer. Thermogravimetric analysis (TGA) was carried out on a TA Q50 system at a heating rate of 10 °C min^{-1} under a nitrogen atmosphere. Variable-temperature magnetic susceptibility, zero-field ac magnetic susceptibility, and field dependence of magnetization were measured on a Quantum Design MPMS-XL5 (SQUID) magnetometer. Diamagnetic corrections were estimated from Pascal's constants for all constituent atoms.

Synthesis of 1

A mixture of Mn(CH₃COO)₂·4H₂O (0.30 mmol), H₂L (0.32 mmol) and urea (0.38 mmol) in 10 mL distilled water was sealed in a Parr Teflon-lined autoclave (23 mL) and heated at 150 °C for 3 days. The final pH value was about 5.5 and colourless plate-shaped crystals of **1** were collected in ca. 55% yield based on Mn. The purity of the as-grown crystals was confirmed by PXRD (Fig. S1a, ESI†). IR data (KBr, cm^{-1}; see Fig. S3, ESI†): 3649(m), 3426(m), 3074(m), 3049(m), 2907(m), 2360(m), 1586(vs), 1415(s), 1299(m), 1190(m), 1147(s), 1122(s), 1034(s), 1134(s), 956(m), 925(m), 764(m), 729(m), 699(m), 634(m), 601(m), 529(s), 495(m).

Synthesis of 2

A mixture of CoCl₂·6H₂O (0.30 mmol), H₂L (0.32 mmol) and urea (0.30 mmol) in 10 mL distilled water was sealed into a Parr Teflon-lined autoclave (23 mL) and heated at 150 °C for 3 days. The final pH value was about 5.0 and pink plate-shaped crystals of **1** were collected in ca. 85% yield based on Co. The purity of the as-grown crystals was confirmed by PXRD (Fig. S1b, ESI†). IR data (KBr, cm^{-1}; see Fig. S3, ESI†): 3448(s), 3071(m), 2968(m), 2816(m), 2659(m), 2376(m), 1632(vs), 1595(s), 1516(m), 1387(m), 1349(s), 1114(s), 1044(m), 730(m), 646(m), 538(m).

Single-crystal structure determination

Data collections for **1** and **2** were performed on a Smart ApexII CCD diffractometer equipped with a graphite-monochromated Mo-Kα radiation source (λ = 0.71073 Å).

Their intensity data were collected at 296 K. The data sets were corrected for Lorentz and polarization factors as well as for absorption by the SADABS program.[13] Crystal structures were solved by direct methods and refined by full-matrix least-squares fitting on F^2 with the SHELXTL program package.[14] The final difference Fourier maps for **1** showed the highest residual peak of 1.41 e Å^{-3} (1.01 Å from the Mn1 atom) and the deepest hole of −0.99 e Å^{-3} (0.67 Å from the H2A atom). The residuals for **2** (0.68 and −0.65 e Å^{-3}) are quite small. C-bound H atoms were generated geometrically while O-bound H atoms were located in the difference Fourier map. All non-hydrogen atoms were refined with anisotropic thermal parameters, whereas all hydrogen atoms were refined isotropically. Crystallographic data and structural refinements for **1** and **2** are summarized in Table 1. Selected bond lengths are listed in Table 2. More details on the crystallographic studies as well as atom displacement parameters are given in the X-ray crystallographic files in CIF format.

Results and discussion

Synthesis and thermogravimetric analysis

The syntheses of **1** and **2** were carried out using a hydrothermal process in the presence of urea, which slowly hydrolyses at the temperature of the reaction, releasing ammonia and slowly raising the pH of the solution. Their thermal stability was examined by TGA under a nitrogen atmosphere, showing that **1** and **2** are stable up to 325 and 303 °C, respectively, whereupon they start decomposing (Fig. S2, ESI†).

Description of the crystal structure

Compounds **1** and **2** crystallize in the monoclinic space group $P2_1/n$ and they are isomorphous in structure, hence only the structure of **1** will be discussed in detail as a representative. The asymmetric unit of **1** contains two types of Mn^{2+} ions, one L^{2-} ligand, and one OH$^-$ group. The +2 oxidation state of the manganese ions was confirmed by bond valence sum (BVS) analysis (1.995 for the Mn1 ion and 2.062 for the Mn2 ion).[15] While the Mn1 ion lying on a general

Table 1 Summary of crystal data and structural refinements for **1** and **2**

Compound	1	2
Empirical formula	C₁₈H₂₀O₁₀P₂Mn₃	C₁₈H₂₀O₁₀P₂Co₃
Formula weight	623.10	635.07
Space group	$P2_1/n$	$P2_1/n$
a (Å)	5.6315(4)	5.4625(4)
b (Å)	6.7154(5)	6.5901(6)
c (Å)	29.169(3)	29.293(3)
β/deg	91.174(6)	90.889(6)
V/Å³	1102.88(16)	1054.38(15)
Z	2	2
D_{calcd}/g cm^{-3}	1.876	2.000
μ/mm^{-1}	1.890	2.541
GOF on F^2	1.083	1.001
R_1, wR_2 [$I > 2\sigma(I)$]^a	0.0887, 0.1933	0.0414, 0.0824
R_1, wR_2 (all data)	0.1072, 0.2018	0.0603, 0.0895

^{a} $R_1 = \sum||F_o| - |F_c||/\sum|F_o|$, w$R_2 = \{\sum w[(F_o)^2 - (F_c)^2]^2/\sum w[(F_o)^2]^2\}^{1/2}$.
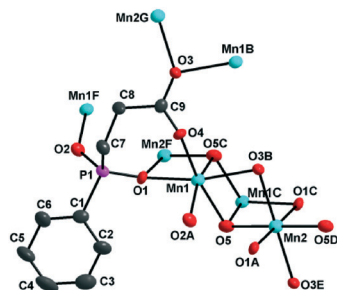
Table 2 Selected bond lengths (Å) for **1** and **2**

1

Mn(1)–O(2)#1	2.138(6)	Mn(1)–O(5)#2	2.156(6)
Mn(1)–O(4)	2.168(7)	Mn(1)–O(5)	2.217(7)
Mn(1)–O(1)	2.258(6)	Mn(1)–O(1)#3	2.268(6)
Mn(2)–O(5)	2.097(6)	Mn(2)–O(3)#3	2.213(6)
Mn(2)–O(1)#1	2.266(7)		

2

Co(1)–O(2)#1	2.054(2)	Co(1)–O(5)#2	2.058(2)
Co(1)–O(4)	2.096(3)	Co(1)–O(5)	2.136(3)
Co(1)–O(3)#3	2.171(3)	Co(1)–O(1)	2.224(3)
Co(2)–O(5)	2.009(3)	Co(2)–O(3)#3	2.138(2)
Co(2)–O(1)#1	2.172(2)		

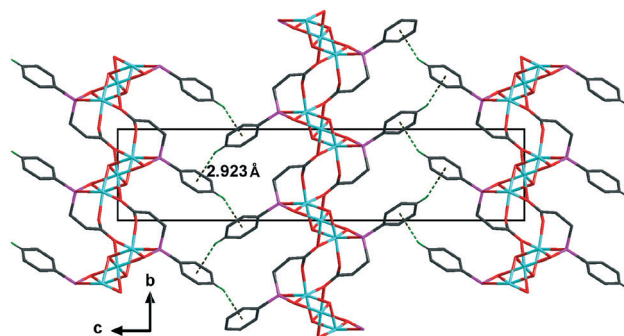Symmetry codes: #1 x − 1, y, z; #2 −x + 1, −y + 1, −z; #3 −x + 1, −y, −z.

Fig. 2 View of the layered structure of **1** down the *c*-axis. Phenyl groups of the L^{2-} ligands and all hydrogen atoms have been omitted for clarity. For other display details, see Fig. 1.

position is octahedrally coordinated by two OH$^-$ ligands, two phosphinate O atoms and two carboxylate O atoms of three L^{2-} ligands, the Mn2 ion located at an inversion centre is half-occupied and octahedrally coordinated by two symmetry-related OH$^-$ groups as well as two phosphinate O atoms and two carboxylate O atoms from two pairs of symmetry-related L^{2-} ligands (Fig. 1). The Mn–O distances (2.097(6)–2.268(6) Å) are in the normal range (Table 1). The unique L^{2-} ligand adopts a [5.2$_{12}$1$_3$2$_{45}$1$_1$] coordination mode according to the Harris notation.[16] By utilizing all of its four O donors, it chelates one Mn^{2+} ion and bridges four other Mn^{2+} ions, with one phosphinate O atom and one carboxylate O atom acting as μ$_2$-O bridges, respectively (Fig. 1). For **2**, a similar coordination mode can be observed, except that the Co–O distances (2.009(3)–2.224(3) Å) are slightly shorter than the Mn–O distances of **1**. The +2 oxidation state of the cobalt ions was also confirmed by BVS analysis (1.897 for the Co1 ion and 1.995 for the Co2 ion).

The interconnection of the Mn^{2+} ions by the L^{2-} and μ$_3$-OH$^-$ ligands results in the formation of a complicated layered structure. As shown in Fig. 2, one Mn2 and two equivalent Mn1 ions are connected by the μ$_3$-OH$^-$ group, forming a Mn$_3$(μ$_3$-OH) triangle unit. In such a triangle unit, the Mn···Mn distances (Å) are 3.4407(2) for Mn1···Mn1A, 3.2520(2) for Mn1···Mn2, and 3.3468(2) for Mn1A···Mn2, respectively. The

Mn1–O5–Mn1A, Mn1–O5–Mn2 and Mn1A–O5–Mn2 angles (°) are 103.762(2), 97.790(2) and 103.783(2), respectively. The Mn1···Mn2 and Mn1A···Mn2 edges are also bridged by the carboxylate oxygen (O3) and phosphinate oxygen (O1A) of the L^{2-} ligand, respectively. The corresponding Mn1–O3–Mn2 and Mn1A–O1A–Mn2 angles (°) are 93.053(2) and 95.419(2), respectively. The neighbouring Mn$_3$(μ$_3$-OH) triangle units are both corner-shared at the Mn2 site and edge-shared at the Mn1···Mn1A borderline, thus leading to an infinite Δ-type chain running along the *a*-axis (Fig. 2, top). The neighbouring chains are further bridged by the Y-shaped "–(CH$_2$)$_2$–C(–O–)–" spacers to form a layer in the *ab* plane. The shortest inter-chain Mn···Mn distance within the layer is 4.6801(3) Å.

Furthermore, the layers in **1** are assembled through C–H···π interactions between the phenyl groups of the L^{2-} ligands at two adjacent layers, forming a three-dimensional supramolecular structure (Fig. 3). The inter-layer distance is 14.929(1) Å.

Magnetic property studies

The temperature-dependent magnetic susceptibility was measured at 1000 Oe in the range of 1.8 (2.0)–300 K on crushed crystalline samples of **1** and **2**.

Fig. 1 ORTEP representation of the selected unit of **1**. The anisotropic displacement ellipsoids are drawn at 50% probability. Symmetry codes for the generated atoms: A. −1 + *x*, *y*, *z*; B. 1 − *x*, −*y*, −*z*; C. 1 − *x*, 1 − *y*, −*z*; D. −*x*, 1 − *y*, −*z*; E. −1 + *x*, 1 + *y*, *z*; F. 1 + *x*, *y*, *z*; G. 1 + *x*, −1 + *y*, *z*.

Fig. 3 View of the three-dimensional supramolecular structure of **1** down the *a*-axis. All hydrogen atoms except for the H4A atom have been omitted for clarity. The C–H···π interactions between the inter-layer L^{2-} ligands are drawn as dashed lines. The dihedral angle of two adjacent inter-layer phenyl rings is *ca.* 75.4°. For other display details, see Fig. 1.

For **1**, the $\chi_m T$ value for a Mn$_3$ triangle unit at 300 K is 12.1 cm^3 mol^{-1} K, which is smaller than the spin-only value for three Mn(II) ions (S = 5/2, 13.12 cm^3 mol^{-1} K for g = 2.0). With decreasing temperature, the $\chi_m T$ value first decreases gradually to a minimum value of *ca.* 5.85 cm^3 mol^{-1} K at 18 K, then increases sharply to a maximum value of 34.2 cm^3 mol^{-1} K at 4 K, and finally drops down to 26.0 cm^3 mol^{-1} K at 2 K (Fig. 4a). The data at 30–300 K can be fitted to the Curie–Weiss law, giving C = 13.61 cm^3 mol^{-1} K and θ = −34.0 K. The negative θ value indicates that there are dominant antiferromagnetic interactions between the Mn(II) ions. On the other hand, the increase of the $\chi_m T$ value below 18 K implies the uncompensating magnetic moment owing to the spin-frustrated/spin-competing interaction in μ$_3$-OH$^-$-bridged Mn$_3$ units; whereas, the decrease of the $\chi_m T$ value below 4 K is likely due to a saturation effect (*vide infra*) and/or a weak interchain antiferromagnetic interaction.

The field dependence of the magnetization at 2.0 K is shown in Fig. 4b. The magnetization curve shows a rapid increase at very small external fields, and then exhibits a linear increase at the high-field range. The value (4.82 $N\beta$) at 5 T per Mn$_3$ unit is close to the moment of one Mn(II) ion (5 $N\beta$), suggesting a non-compensating resultant moment of one

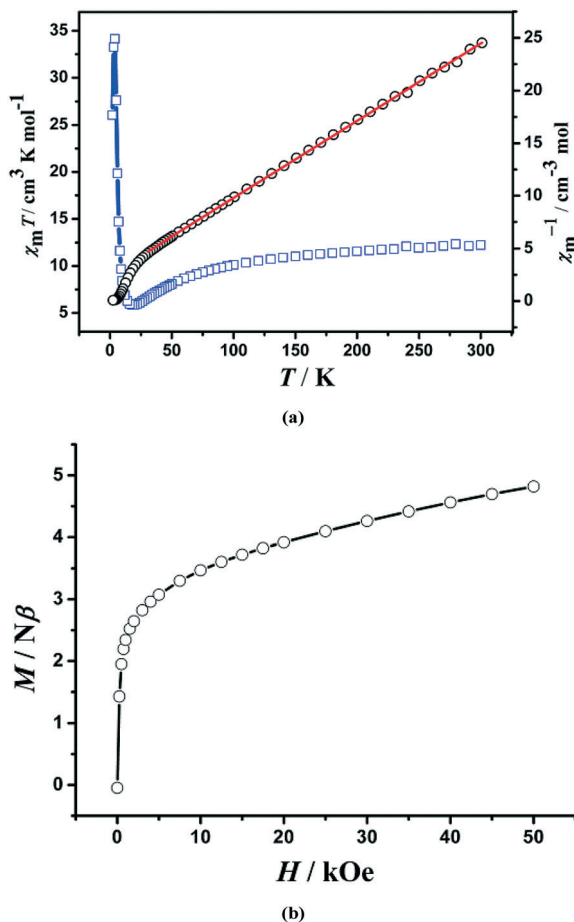Mn(II) ion per Mn$_3$ unit, a typical characteristic of topological ferrimagnets.[17] No significant remnant magnetization and coercive field were observed in the hysteresis loop at 2.0 K, suggesting a soft magnetic characteristic for **1** (Fig. S4, ESI†). Moreover, the FC and ZFC curves diverge at below 3.6 K (Fig. S5, ESI†), suggesting the occurrence of irreversibility of magnetization. AC susceptibility measurements revealed that both in-phase (χ') and out-of-phase (χ'') signals (Fig. S6, ESI†) are somewhat frequency-dependent, which should be ascribed to spin-glass behaviours that often happen on triangle spin-competing systems.[18]

The complicated magnetic behaviour at low temperature should be mainly ascribed to the complicated magnetic exchange topology in **1**. As shown in Fig. 2, a Δ-type chain is built from alternating corner- and edge-sharing Mn$_3$(μ$_3$-OH) triangles with the carboxylate and phosphinate as co-bridges. As revealed by temperature susceptibilities at high temperature, the intra-triangle magnetic interaction should be of antiferromagnetic type, which is consistent with the Mn–O–Mn angles in the range of 92.9(3)–103.9(4)°. In such a Δ-type chain, spin competition is expected as the intrachain magnetic interactions cannot be satisfied at the same time (Fig. 5). This spin-competing behaviour is also supported by a moderate value of the frustration parameter (f = $|\theta|/T_N$ = 9.2) in **1**.[19] As the Mn(II) ion usually has a weak magnetic anisotropy, the magnetic structure in such a Δ-type chain is strongly determined by the coupling between the sites. For this case, a single phase transition from the paramagnetic state to a magnetically ordered state was predicted.[20] Taking into consideration the large $\chi'T$ value (131 cm^3 mol^{-1} K) observed at 3.8 K and the magnetization of 4.82 $N\beta$ at 5 T, one of the possible magnetic structures of a single chain at low temperature can be proposed for **1**. As shown in Fig. 6, for each single chain, the moments on the edge-sharing (Mn1) and vertex-sharing (Mn2) sites form two individual sub-lattices, which are anti-parallel to each other, and thus, a non-compensating resultant moment of one Mn(II) ion per Mn$_3$ unit could be formed, leading to a topologically ferrimagnetically ordered state for **1**.

For **2**, the $\chi_m T$ value at room temperature is 9.63 cm^3 mol^{-1} K, which is much larger than the expected spin-only value (5.625 cm^3 mol^{-1} K) for three magnetically isolated Co(II) ions (S = 3/2, g = 2) and this phenomenon can be attributed to the strong spin–orbit coupling of Co(II) ions. As the temperature decreases, the value of $\chi_m T$ slowly decreases at high temperature and quickly decreases down to a minimum value of 0.48 cm^3 mol^{-1} K at 2.0 K. Curie–Weiss fitting of the

Fig. 4 (a) Temperature dependence of $\chi_m T$ (□) and χ_m^{-1} (○) for the microcrystalline sample of **1**. The red solid line is Curie–Weiss fitting; (b) magnetization measured at 2 K for **1**.
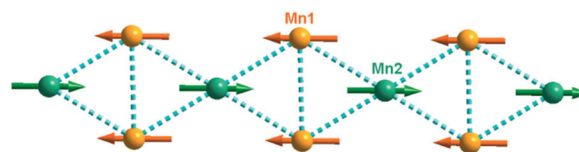

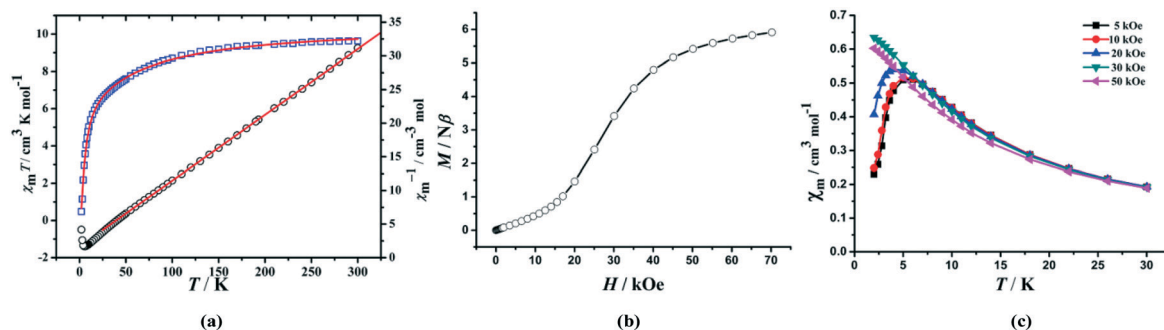**Fig. 5** A proposed arrangement of the magnetic moments in a single chain of **1**.

Fig. 6 (a) Temperature dependence of $\chi_m T$ ($\square$) and χ_m^{-1} ($\circ$) measured at 1 kOe for the microcrystalline sample of **2**. The red solid lines represent the best non-linear fitting and Curie–Weiss fitting; (b) the plot of M *vs. H* measured at 2 K; (c) the plots of χ_m *vs. T* below 30 K at different applied fields.

magnetic data from 2 K to 300 K for **2** results in C = 10.23 cm^3 mol^{-1} K and θ = −17.3 K. Notably, the negative θ value does not indicate dominant antiferromagnetic coupling between the metal centers because of the strong spin–orbit coupling of Co(II) ions, which itself can lead to a negative θ value and a decrease of $\chi_m T$ at high temperature.[21] The strength of the antiferromagnetic exchange interaction caused by the spin–orbit coupling of Co(II) at high temperature was estimated based on eqn (1).[22]

$$\chi T = A \exp(-E_1/kT) + B \exp(-E_2/kT) \tag{1}$$

In eqn (1), $A + B$ equals the Curie constant, and E_1 and E_2 are the spin–orbit coupling constant and activation energy of antiferromagnetic interactions, respectively. The best fit of the experimental data gives $A + B$ = 10.53 cm^3 mol^{-1} K, $-E_1/k$ = −90.24 K, and $-E_2/k$ = −4.98 K for **2** (Fig. 6a). The negative value of $-E_2/k$ indicates the dominant antiferromagnetic interactions between adjacent Co(II) ions.[22]

The field-dependent magnetization of **2** at 2 K has a value of 5.92 $N\beta$ (far from the saturation value) at 7 T and exhibits a pronounced sigmoid shape at low field. The latter implies spin fluctuation behaviour for **2** that a magnetic transition occurs from the AF interaction at low field to a FM state at high field (Fig. 6b), and the critical field defined as dM/dH at 2 K is 25 kOe. To investigate the nature of the spin fluctuation of **2**, the low temperature magnetic susceptibilities at different fields were measured. The χ_m *vs. T* plot (Fig. 6c) shows a cusp around 5.0 K when the applied fields are lower than 25 kOe. Below 5.0 K, χ_m drops sharply toward zero, suggesting that the ground state of the system is S = 0. The cusp disappears at higher fields and the antiferromagnetic couplings mediated by μ_3-OH could be overcome at external fields larger than 25 kOe, from which **2** turns into a ferromagnetic state. In addition, the antiferromagnetic behavior is further confirmed by the temperature-dependent in-phase (χ') magnetic susceptibilities (Fig. S7, ESI†), but no out-of-phase (χ'') signals could be observed.

As is known, the usual coordination modes of carboxylates to transfer magnetism could be divided into four types: two of which are *syn–syn*-μ_2-η^1:η^1 and *anti–anti*-μ_2-η^1:η^1 modes, which

likely produce antiferromagnetism between Co^{II} ions; one is a *syn–anti*-μ_2-η^1:η^1 mode, which probably produces weak ferromagnetism; the last one is a μ_2-η^2 mode, which provides more opportunities for generating ferromagnetism.[21b] A common rule that they transfer ferromagnetic interactions when the Co–O–Co angle is smaller than 110° was widely recognized. For **2**, there exists an *anti–syn–anti*-μ_3-η^1:η^2 mode of carboxylate groups, phosphinate and μ_3-OH$^-$. The Co–O–Co angles of 93.54° and 94.51° (O atoms are from phosphinate and carboxylate) and *anti–syn–anti*-μ_3-η^1:η^2 carboxylates are favorable for the transference of ferromagnetism, however, the existence of a μ_3-OH$^-$ magnetic exchange pathway may play a key role in the antiferromagnetic interaction between Co^{II} ions.

Conclusions

In summary, we report the first example of metal carboxylate–phosphinates with the μ_3-OH$^-$ bridge featuring magnetic Δ-chains. Magnetic studies on such compounds show that there are dominant antiferromagnetic interactions between the Mn(II) ions and the Co(II) ions. Moreover, the complicated magnetic exchange topology results in spin competition in **1**, showing spin-glass behaviours. Complex **2** exhibits spin fluctuation behaviours with the critical field of 25 kOe at 2 K. Further research work is in progress to explore other μ_3-O-bridged coordination polymers exhibiting various magnetic Δ-chains.

Acknowledgements

Notes and references

1 O. Kahn, *Molecular Magnetism*, VCH, Weinheim, Germany, 1993; D. Gatteschi, R. Sessoli and J. Villian, *Molecular Nanomagnets*, Oxford University Press, Oxford, 2006.

2 (a) M. Sakamoto, K. Manseki and H. Ōkawa, *Coord. Chem. Rev.*, 2001, **219–22**, 379–414; (b) M. N. Leuenberger and D. Loss, *Nature*, 2001, **410**, 789; (c) D. Gatteschi and R. Sessoli, *Angew. Chem., Int. Ed.*, 2003, **42**, 268–297.

3 (a) R. E. P. Winpenny, *Angew. Chem., Int. Ed.*, 2008, **47**, 7992–7994; (b) L. Bogani and W. Wernsdorfer, *Nat. Mater.*, 2008, **7**, 179–186.

4 (a) L. Balents, *Nature*, 2010, **464**, 199–208; (b) F. H. Aidoudi, D. W. Aldous, R. J. Goff, A. M. Z. Slawin, J. P. Attfield, R. E. Morris and P. Lightfoot, *Nat. Chem.*, 2011, **3**, 801–806; (c) Y.-M. Li, C.-Y. Xiao, X.-D. Zhang, Y.-Q. Xu, H.-J. Lun and J.-Y. Niu, *CrystEngComm*, 2013, **15**, 7756–7762.

5 (a) J. J. Borrás-Almenar, E. Coronado, C. J. Gómez-Garcia, R. Georges and C. Muñz-Roca, *Chem. Phys. Lett.*, 1991, **186**, 410–414; (b) J. J. Borrás-Almenar, E. Coronado, J. C. Gallart, R. Georges and C. J. Gómez-Garcia, *J. Magn. Magn. Mater.*, 1992, **104–107**, 835–836.

6 (a) C. Ruiz-Pérez, M. Hernández-Molina, P. Lorenzo-Luis, F. Lloret, J. Cano and M. Julve, *Inorg. Chem.*, 2000, **39**, 3845–3852; (b) S. O. H. Gutschke, D. J. Price, A. K. Powell and P. T. Wood, *Angew. Chem., Int. Ed.*, 2001, **40**, 1920–1923; (c) S. M. Humphrey and P. T. Wood, *J. Am. Chem. Soc.*, 2004, **126**, 13236–13237; (d) H. Kikuchi, Y. Fujii, M. Chiba, S. Mitsudo and T. Idehara, *Polyhedron*, 2005, **24**, 2835–2838; (e) X.-N. Cheng, W.-X. Zhang, Y.-Z. Zheng and X.-M. Chen, *Chem. Commun.*, 2006, 3603–3605.

7 (a) X.-N. Cheng, W. Xue and X.-M. Chen, *Eur. J. Inorg. Chem.*, 2010, 3850–3855; (b) E.-C. Yang, Z.-Y. Liu, X.-Y. Wu and X.-J. Zhao, *Chem. Commun.*, 2011, **47**, 8629–8631; (c) Y.-Q. Wang, X.-M. Zhang, X.-B. Li, B.-W. Wang and E.-Q. Gao, *Inorg. Chem.*, 2011, **50**, 6314–6322; (d) W.-C. Song, J. Tao, T.-L. Hu, Y.-F. Zeng and X.-H. Bu, *Dalton Trans.*, 2011, **40**, 11955–11959; (e) D. S. Liu, Y. Sui, T. W. Wang, C. C. Huang, J. Z. Chen and X. Z. You, *Dalton Trans.*, 2012, **41**, 5301–5306; (f) R.-X. Yao, Y.-L. Qin, F. Ji, Y.-F. Zhao and X.-M. Zhang, *Dalton Trans.*, 2013, **42**, 6611–6618; (g) Z.-S. Cai, S.-S. Bao, M. Ren and L.-M. Zheng, *Chem. – Eur. J.*, 2014, **20**, 17137–17142.

8 (a) Q. Yu, Y.-F. Zeng, J.-P. Zhao, Q. Yang, B.-W. Hu, Z. Chang and X.-H. Bu, *Inorg. Chem.*, 2010, **49**, 4301–4306; (b) A. Das, G. M. Rosair, M. Salah El Fallah, J. Ribas and S. Mitra, *Inorg. Chem.*, 2006, **45**, 3301–3306.

9 (a) P. S. Mukherjee, S. Dalai, E. Zangrando, F. Lloretc and N. R. Chaudhuri, *Chem. Commun.*, 2001, 1444–1445; (b) T. Liu, Y. Zhang, Z. Wang and S. Gao, *Inorg. Chem.*, 2006, **45**, 2782–2784.

10 (a) Y.-H. Sun, X. Xu, Z.-Y. Du, L.-J. Dong, C.-C. Zhao and Y.-R. Xie, *Dalton Trans.*, 2011, **40**, 9295–9298; (b) L.-J. Dong, C.-C. Zhao, X. Xu, Z.-Y. Du, Y.-R. Xie and J. Zhang, *Cryst. Growth Des.*, 2012, **12**, 2052–2058; (c) C.-C. Zhao, Z.-G. Zhou,

X. Xu, L.-J. Dong, G.-H. Xu and Z.-Y. Du, *Polyhedron*, 2013, **51**, 18–26; (d) C.-C. Zhao, J.-W. Zhang, Z.-G. Zhou and Z.-Y. Du, *J. Mol. Struct.*, 2013, **1033**, 253–257; (e) Y.-P. Zhao, J.-W. Zhang, C.-C. Zhao and Z.-Y. Du, *Inorg. Chim. Acta*, 2014, **414**, 121–126.

11 (a) W. Yang, H. Wang, W.-G. Tian, J. Li and Z.-M. Sun, *Eur. J. Inorg. Chem.*, 2014, 5378–5384; (b) L. Guan, H.-F. Sheng and Y. Wang, *Phosphorus, Sulfur Silicon Relat. Elem.*, 2015, **190**, 372–379; (c) J. Li, C.-C. Xue, S. Liu and Z.-X. Wang, *Solid State Sci.*, 2016, **61**, 111–115; (d) Z.-Y. Du, H.-R. Wen, C.-M. Liu, Y.-H. Sun, Y.-B. Lu and Y.-R. Xie, *Cryst. Growth Des.*, 2010, **10**, 3721–3726.

12 G. H. Birumand and R. F. Jansen, *U.S. Pat.*, 4081463, 1978. See also: http://www.google.com/patents/US4081463.

13 Bruker, *APEX2, SADABS and SAINT*, Bruker AXS Inc., Madison, Wisconsin, USA, 2008.

14 G. M. Sheldrick, *SHELX-96 Program for Crystal Structure Determination*, 1996.

15 N. E. Brese and M. O'Keeffe, *Acta Crystallogr., Sect. B: Struct. Sci.*, 1991, **47**, 192–197.

16 R. A. Coxall, S. G. Harris, D. K. Henderson, S. Parsons, P. A. Tasker and R. E. P. Winpenny, *J. Chem. Soc., Dalton Trans.*, 2000, 2349–2356.

17 (a) M. A. M. Abu-Youssef, M. Drillon, A. Escuer, M. A. S. Goher, F. A. Mautner and R. Vicente, *Inorg. Chem.*, 2000, **39**, 5022–5027; (b) M.-H. Zeng, M.-C. Wu, H. Liang, Y.-L. Zhou, X.-M. Chen and S.-W. Ng, *Inorg. Chem.*, 2007, **46**, 7241–7243; (c) J.-Y. Zou, W. Shi, N. Xu, L.-L. Li, J.-K. Tang, H.-L. Gao, J.-Z. Cui and P. Cheng, *Chem. Commun.*, 2013, **49**, 8226–8228.

18 C.-M. Liu, D.-Q. Zhang and D.-B. Zhu, *Chem. Commun.*, 2008, 368–370.

19 (a) J. L. Manson, E. Ressouche and J. S. Miller, *Inorg. Chem.*, 2000, **39**, 1135–1141; (b) S. H. Lee, C. Broholm, C. Ratcliff, G. Gasparovic, Q. Huang, T. H. Kim and S. W. Cheong, *Nature*, 2002, **418**, 856–858; (c) A. Harrison, *J. Phys.: Condens. Matter*, 2004, **16**, S553–S572.

20 (a) R. A. Mole, J. A. Stride, P. L. F. Henry, M. Hoelzel, A. Senyshyn, A. Alberola, C. J. G. Garcia, P. R. Raithby and P. T. Wood, *Inorg. Chem.*, 2011, **50**, 2246–2251; (b) R. A. Mole, M. A. Nadeem, J. A. Stride, V. K. Peterson and P. T. Wood, *Inorg. Chem.*, 2013, **52**, 13462–13468.

21 (a) C. Y. Niu, X. F. Zheng, X. S. Wan and C. H. Kou, *Cryst. Growth Des.*, 2011, **11**, 2874–2888; (b) S.-J. Liu, L. Xue, T.-L. Hu and X.-H. Bu, *Dalton Trans.*, 2012, **41**, 6813–6819; (c) D. R. Xiao, G. J. Zhang, J. L. Liu, L. L. Fan, R. Yuan and M. L. Tong, *Dalton Trans.*, 2011, 5680–5683.

22 Q. C. Chu, Z. Su, J. Fan, T. A. Okamura, G. C. Lv, G. X. Liu, W. Y. Sun and N. Ueyama, *Cryst. Growth Des.*, 2011, **11**, 3885–3894.